

NUMERICAL STUDY OF EFFUSION COOLING FLOW AND HEAT TRANSFER

M. WALTON¹ & Z. YANG²

¹Department of Aeronautical and Automotive Engineering, Loughborough University, UK.

²Department of Engineering and Design, University of Sussex, UK.

ABSTRACT

An isothermal and non-isothermal numerical study of effusion cooling flow and heat transfer is conducted using a Reynolds-averaged Navier–Stokes (RANS) approach. A Reynolds stress transport (RST) turbulence model is used to predict the flow field of a staggered array of 12 rows of effusion holes, each hole inclined at 30° to the flat plate. The Reynolds number based on the hole diameter and jet exit velocity is 3800. The blowing ratio in both studies is 5. A conjugate heat transfer approach is adopted in the non-isothermal simulation. For the isothermal case, the RST model is shown to be capable of predicting the injection, penetration, downstream decay and lateral mixing of the effusion jets reasonably well. In addition, the numerical model captures the existence of two counter-rotating vortices emanating from each hole, which causes the entrainment of combustor flow towards the surface of the plate at the leading edge and downstream, influences the mixing of accumulated coolant flow, providing a more uniform surface temperature across the plate. The presence and characteristics of these vortices are in good agreement with previously published research. In the non-isothermal case, the laterally averaged cooling effectiveness across the plate is under-predicted but the trend conforms to that exhibited during experimentation.

Keywords: Conjugate heat transfer, effusion cooling, RANS, RST turbulence model.

1 INTRODUCTION

Gas turbine engines operate at extremely high temperatures; thus, components such as combustion chamber walls, turbine endwalls, turbine blades and shrouds need to be cooled. The desire to increase the efficiency, i.e. reducing the specific fuel consumption and raising the thrust-to-weight ratio of gas turbines, has led to an increase in pressure and temperature in the combustion chamber and turbine. The operational life of the combustion chamber walls decreases as the temperature increases; thus, a method of cooling must be used to protect the wall. Whilst wall cooling is essential, there is also a need to minimise the proportion of air used for cooling as air taken away from the combustion process increases nitrous oxide emissions. Amongst many techniques available, effusion cooling, also known as full coverage film cooling (FCFC), is considered the most practical. In this approach, cooler air, usually bled from the latter stages of the compressor, is injected from the combustor outer casing side through thousands of sub-millimetric angled perforations and enters the boundary layer on the internal wall of the combustor. The cooling film that protects the liner from the hot gases results from the coalescence of the discrete micro-jets emanating from the perforations.

Engineers are always trying to extract greater cooling performance from less cooling air whilst also trying to maximise the overall film-cooling effectiveness so that the amount of air used for cooling can be reduced. A fundamental understanding of the mechanisms involved in effusion flow fields is therefore required to make significant advances in cooling technology. At the same time, designers need a predictive design tool that allows quick turnaround times without the current build and break approach. The RANS approach within the framework of computational fluid dynamics (CFD) presents the designer with the potential for an effective, fast and relatively accurate method of achieving this.

Since effusion cooling is known to have drastic effects on the whole flow structure, an appropriate model is needed for numerical approaches to reproduce the effect of effusion cooling on the main flow with a reasonable computational cost. To be useful in practical RANS computations, any FCFC model should relate the fluxes through the effusion plate at a given position to the outer flow quantities at the same position, on both the suction (coolant) and the injection (combustor) sides. Despite numerous studies dealing with FCFC, data relating wall fluxes to suction and injection quantities are unusual. The suction of a boundary layer through one or several perforations is not highly documented [1], and the flow at the suction side is rarely considered in detail in the studies concerning injection through short holes [2].

Walters and Leylek [3] emphasised the importance of reproducing the exact geometry for effusion cooling studies. However, generating relevant data experimentally is very challenging; the high temperatures and pressures in the combustion chambers are difficult to reproduce in test rigs, and experimental techniques are rarely adapted to such conditions. Moreover, as the micro-jets are sub-millimetric in size, the main flow features are out of reach of current measurements techniques. This explains the lack of detailed measurements in realistic operating conditions. Accurate information about the velocity field in FCFC configurations is current only available on large-scale isothermal plates. Very often, only small temperature differences between the hot and the cold streams are investigated [4–6].

There are also many parameters related to the cooling performance of effusive cooling: hole shape, spacing and angle, blowing ratio, free stream turbulence intensity and the thermal conductivity, etc. Martinez-Botas and Yuen [7] measured heat transfer coefficient and adiabatic effectiveness of a variety of geometries in a flat plate to test the influence of the injection angle by varying blowing ratio from 0.33 to 2.0. Lin *et al.* [8] carried out both experimental and numerical studies of adiabatic film cooling effectiveness of four different 30° inclined multi-hole film cooling configurations. Facchini *et al.* [9] measured the overall effectiveness and the heat transfer coefficient at variable blowing ratios on a real engine cooling scheme to evaluate the combined effects of slot, effusion, and a large dilution hole. Ligiani *et al.* [10] experimentally investigated the effects of dense and sparse hole arrays at different blowing ratios on film effectiveness and heat transfer coefficients. Andreini *et al.* [11] performed an experiment to study the density ratio effects on the cooling performance of a combined slot/effusion combustor cooling system. A very recent review about effusion cooling was given by Krewinkel [12] in which several important aspects were addressed including the basic geometric and aerodynamic parameters known from film-cooling, the thermal conductivity of the base material, simplified approaches for modelling effusion-cooling and so on.

Ideally, relevant data to build FCFC models would contain detailed information about the dynamical and thermal behaviours of the flow on both sides of the plate and correspond to a realistic configuration with a large array of holes submitted to non-isothermal conditions. Detailed flow measurements in non-isothermal situations have rarely been performed and the complete configuration has seldom been considered.

In FCFC scenarios, resolving the flow in each of the hundreds or thousands of holes would be very expensive. As long as only a few holes are considered, wall-resolved large eddy simulations (LES) can be performed in place of RANS calculations to gain insight into the jet mainstream interaction. LES of a single jet in cross-flow (JCF) have been performed using periodic boundary conditions in the spanwise direction to mimic a row of cooling jets. Mendez *et al.* [13] developed a numerical methodology (also involving periodic boundary conditions in the spanwise direction) for isothermal and non-isothermal flow conditions, which proved to be successful at predicting the FCFC flow structure. Bennett *et al.* [14] completed an isothermal LES study of oblique patch effusion cooling using a staggered array of

12 rows of effusion holes. The numerical model was shown to be capable of accurately predicting the injection, penetration, downstream decay and coalescence of the effusion jets.

Numerical capabilities have increased in the past two decades allowing two-equation eddy viscosity model (EVM) based simulations of FCFC with many rows to be performed. The issues of modelling error and the non-universality of two-equation turbulence models do not allow one to consider RANS codes as predictive tools in FCFC scenarios. In general, two-equation EVM is unable to predict the near field accurately. The lateral spreading and mixing of the film-cooling jets are underpredicted [15–17] and the vertical penetration is overpredicted. The lower lateral spreading is linked to underestimation of the eddy viscosity in the lateral direction.

The crucial mechanism misrepresented by any linear EVM is turbulence anisotropy and related to it, the attenuation or amplification of turbulence due to curvature-related strain. A more advanced model is therefore required that can accurately predict the distribution of Reynolds stresses whilst having a lower computational burden than current LES techniques. The solution is the RST turbulence model.

Very few FCFC simulations involving the use of the RST model have been performed. Jansson and Davidson [18] simulated mean velocity profiles and cooling effectiveness of a single JCF using the $k - \varepsilon$ and RST models. Both models failed to reproduce the correct velocities at $M = 1$, possibly due to the unsteady behaviour of the flow downstream of the jet exits, but even so the RST model proved to be more accurate than conventional two-equation EVM. The cooling effectiveness close to the centre of the jet exit was generally overpredicted and, away from the jet exit in the spanwise direction, the effectiveness was under-predicted. Jansson and Davidson [19] applied near wall corrections to the basic linear model (used in the 1994 simulation) and used a low-Reynolds RST model to predict effusion cooling in a double row discrete hole configuration and reported better predictions than a two-layer $k - \varepsilon$ model.

Gustafsson and Johansson [20] performed three CFD simulations of a slanted JCF and compared the results with detailed 3D Laser Doppler Velocimetry (LDV) measurements. Three turbulence models were compared; the realisable $k - \varepsilon$, $k - \omega$ SST and RST models. The RST model was found to be the most accurate in terms of predicting the mean flow field, Reynolds stresses and mean topology of the velocity field. It was concluded that effusion cooling flow fields with complex 3D turbulent structures requires the use of the RST model.

In this paper, we present and discuss the results of two numerical computations (isothermal and non-isothermal) which use the RST model to simulate the experimental effusion cooling flow work of Scrittore [21]. A densely spaced FCFC array of cooling holes is subjected to isothermal and non-isothermal conditions. In the isothermal study, profiles of streamwise and wall-normal velocity and turbulence level are compared with the experimental data and detailed analysis is given on the flow field. In the non-isothermal study, cooling effectiveness contours and laterally averaged cooling effectiveness across the plate are compared against the experimental data. The topology of the flow is also analysed.

2 GOVERNING EQUATIONS AND COMPUTATIONAL DETAILS

2.1 Governing equations

In contrast to EVMs which calculate the Reynolds stresses by algebraic expressions, RST models calculate the Reynolds stresses by solving a transport equation for each stress components. The transport equations are fairly standard and hence will not be presented here.

Several terms in this exact transport equations need to be modelled. The turbulent diffusive transport term is modelled using a simplified version of the generalised gradient diffusion model proposed by Daly and Harlow [22] to improve stability. The well tested Gibson and Launder pressure-strain model [23] is employed in the current study.

2.2 Computational details

The work completed by Scrittore [21] focussed on obtaining flowfield measurements over a densely spaced full coverage array of film-cooling holes. The plate was subjected to isothermal and non-isothermal conditions. To achieve good spatial resolution the effusion plate (representing the combustor wall) was geometrically scaled by approximately nine times whilst Reynolds number and blowing ratio, $M = \rho_c U_j / \rho_\infty U_\infty$, were matched (ρ_c is the coolant density, ρ_∞ is the mainstream density, U_j is the jet exit velocity and U_∞ is the mainstream velocity). The effusion plate, constructed from urethane foam, comprised 730 cylindrical cooling holes injected at 30° and arranged in 20 rows in the streamwise direction and staggered as illustrated in Fig. 1.

Film-cooling characteristics were studied at four different blowing ratios; 3.2, 3.8, 4.4 and 5.0. The coolant to mainstream density ratio, which is typically quite high in combustors, was not representative in the experiments. Mean velocity profiles in the streamwise (u) and wall-normal (v) directions and the turbulence level were measured one cooling row downstream of rows 1, 5, 10, 15 and 20 for blowing ratios of 3.2 and 5.0. Cooling effectiveness, a dimensionless wall temperature parameter defined as $\eta = (T_\infty - T_w) / (T_\infty - T_c)$ was measured on the effusion test plate for blowing ratios of 3.2 and 5.0 (T_∞ is the mainstream temperature, T_w is the plate wall temperature and T_c is the coolant temperature. The measurement region captured six columns of cooling holes located at the mid-pitch of the test plate, spanning the full range of holes in the streamwise direction).

To minimise computational burden, the domain is reduced to the first 12 rows of holes with periodic boundary conditions imposed in the spanwise direction along the centreline of the column of holes adjacent to the centreline of the plate, mimicking an infinite number of holes across the plate as shown in Fig. 2. Periodicity is not imposed in the streamwise direction since the complex nature of streamwise jet interaction must be captured as fully as possible.

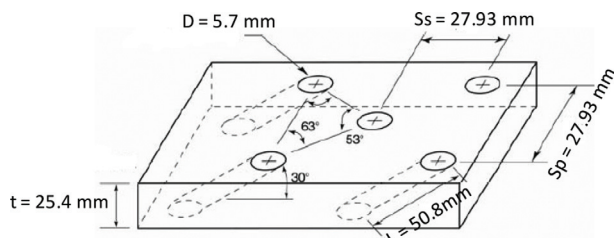


Figure 1: Effusion plate geometry.

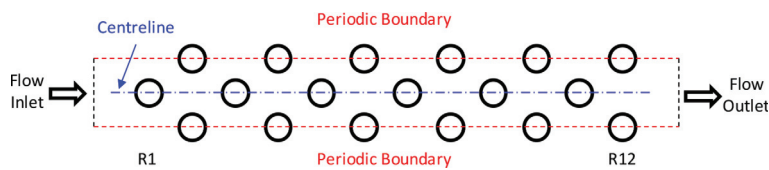


Figure 2: Top view of the computational domain showing effusion holes.

Figure 3 shows the computational domain and the dimensions of the computational domain are defined in Tables 1 and 2. The combustor inlet is positioned five holes diameters upstream of the first row of holes, which coincides with the point at which the inlet velocity profile was measured.

2.3 Boundary conditions

For the isothermal simulation, the measured velocity profile was imposed on the combustor inlet, which is positioned five hole diameters upstream of the first row of holes. A uniform velocity profile was imposed on the cooling plenum inlet; this was determined via a simple mass flow calculation using the hole discharge coefficient of 0.73, the jet hole Reynolds number of 3800 and blowing ratio of 5. All wall boundaries in the domain, including the effusion tubes that connect the combustor and cooling plenum regions, are set to no-slip and adiabatic since no heat transfer takes place. At the combustor outlet, a zero-gradient outflow boundary condition is applied.

Operating conditions for the flow tests consisted of a matched coolant and mainstream temperature of 30°C, resulting in a density ratio of 1. At inlets, both turbulence intensity and

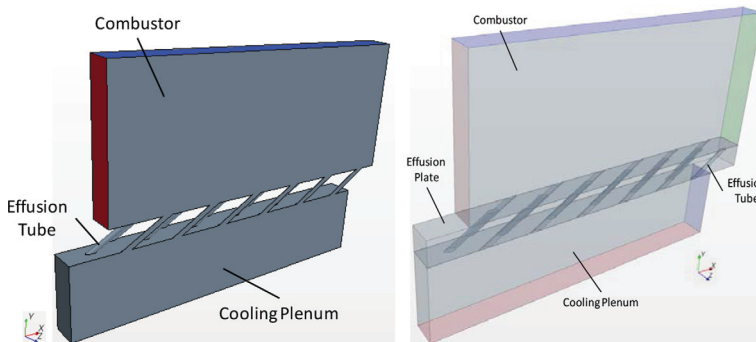


Figure 3: Computational domain: left, isothermal flow; right, non-isothermal case.

Table 1: Dimensions of isothermal computational domain.

	Combustor	Cooling plenum
Width, x (mm)	366.51	363.09
Height, y (mm)	77	150
Depth, z (mm)		27.93

Table 2: Dimensions of non-isothermal computational domain.

	Combustor	Cooling plenum	Effusion plate
Width, x (mm)	366.51	363.09	407.08
Height, y (mm)	77	150	25.4
Depth, z (mm)		27.93	

length scale (based on one hole diameter) are specified; these are 1.3% and 5.7 mm and 2% and 5.7 mm for the combustor and cooling plenum, respectively. The freestream velocity of the combustor is 2.3 and 0.356 m/s at the cooling plenum inlet.

A detailed mesh optimisation study was completed to analyse the use of polyhedral, trimmed and prismatic meshes via two meshing approaches, single region and multi-region meshing and select the optimum mesh for the current effusion scenario. The polyhedral mesh was identified as the most suitable for the current study and three separate grids, coarse grid with 749,564 cells, medium grid with about 1.4 million cells and fine grid with about 1.8 million cells, were generated and it was found that the results obtained using the medium mesh and the fine mesh were very similar with the maximum difference in both the mean velocity and turbulent intensity level <6%. Hence, it was decided that there was no need to refine the mesh further. The final mesh used in the current is shown in Fig. 4; it contains 1,827,858 cells and uses four volumetric controls (VC) (VC1 near combustor wall through to VC4 adjacent to combustor freestream). Each volumetric control is tailored to capture the flow features visible in the experimental streamwise velocity profiles as shown in Fig. 5. The cell sizes for each volumetric control are 0.5 mm in VC1, which gives values of y^+ close to the solid walls about 6 and hence a two-layer approach is employed rather than a traditional wall function for the near wall region, 1 mm in VC2, 2 mm in VC3 and 5.7 mm in VC4. The cell size in the effusion tubes was set to 0.5 mm providing a smooth transition between the volumetric control closest to the combustor bottom wall and the tubes. Cells of 0.5 mm also allows the counter-rotating vortex pair (CVP) in each tube to be resolved accurately, thereby modelling the spreading and mixing of adjacent cooling jets as fully as possible. Two prism layers (total thickness equal to 1 mm) included along the bottom of the combustor wall and the internal walls of each effusion tube allow the complex flow behaviour to be captured accurately.

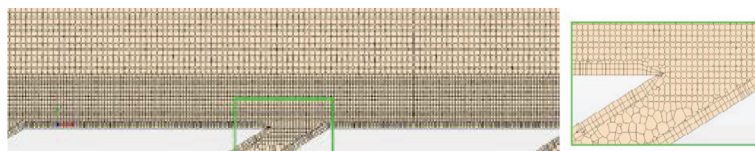


Figure 4: Central plane mesh.

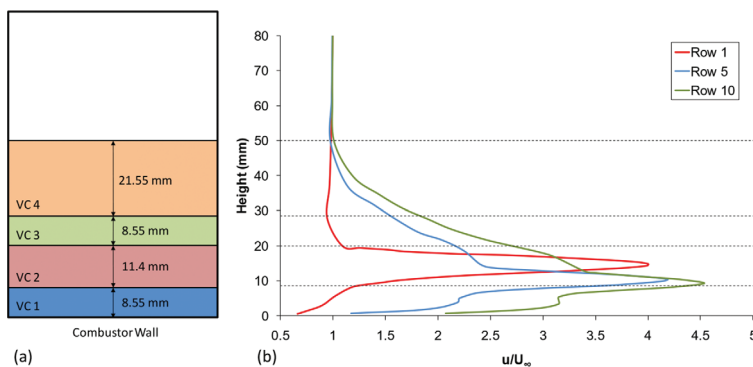


Figure 5: (a) Volumetric control regions and (b) experimental streamwise velocity profiles.

The isothermal simulation was run using a second-order upwind discretisation scheme. The governing flow equations were solved implicitly using a segregated flow model. A co-located variable arrangement (as opposed to staggered) was employed with a Rhie and Chow type pressure–velocity coupling combined with a SIMPLE (Semi-Implicit Method for Predicting Linked Equations) type algorithm.

For the non-isothermal case, effusion cooling has two components to the overall heat transfer; heat transfer as the coolant passes through the wall and the coolant film acting as an insulation layer between the hot gases and the wall. The coupling of these two modes of heat transfer is called conjugate heat transfer (CHT).

As noted from a study by Silietti *et al.* [24], modelling the conductive transfer of heat in the plate is essential to properly capture the heating of the fluid inside each cooling hole; this will inevitably have an effect on the heat transfer coefficient and temperature of the combustor wall and thus how accurately the cooling effectiveness over the combustor wall can be modelled. With this in mind, a CHT approach is adopted to account for heat transfer via plate conduction as well as fluid convection. The combustor, cooling plenum and flow through the holes in the plate is modelled in the same manner as described in the isothermal case with all the dimensions the same except, a solid plate region is now incorporated around the fluid tubes. A non-CHT based set up was also run to quantify the importance of CHT approach.

With the introduction of a solid effusion plate region into the existing isothermal domain, a number of interfaces between the fluid and solid regions are introduced. In the current study, 65 interfaces, 9 of which are periodic (in the spanwise direction), 20 contact interfaces and 36 internal interfaces are used. Internal interfaces, used for fluid-to-fluid regions, were applied between the bottom of the combustor wall and tops of each of the effusion tubes. Internal interfaces were also applied to the top of the cooling plenum and bottom of each of the effusion tubes. Contact interfaces permit CHT between either fluid-to-solid or solid-to-solid regions. This type of interface was applied between the bottom of the combustor wall and the top of the effusion plate, the top of the cooling plenum and bottom of the effusion plate as well as each of the effusion tube walls and the hole walls through the effusion plate. All wall boundaries in the domain were set to no-slip. All walls were set as adiabatic apart from the fluid tube walls, combustor bottom wall and the effusion plate, which were defined with a heat flux equal to 11 W/m^2 [21].

Discretisation and flow conditions remain the same as for the isothermal case except the combustor temperature was 318.15 K with a coolant flow temperature of 299.15 K, resulting in a density ratio of 1.08. Velocity at the cooling plenum inlet is 0.34 m/s and the jet hole exit velocity is calculated at 11.27 m/s. The effusion plate was manufactured from FR-6706 Urethane Foam and as such the following properties were modelled in the CHT approach; thermal conductivity is equal to 0.029 W/m-K , density is equal to 96.11 kg/m^3 and specific heat is equal to 1600 J/kg-K .

3 RESULTS AND DISCUSSION

3.1 Isothermal simulation

Many streamwise velocity, wall-normal velocity and turbulence level profiles, all measured one cooling row downstream of rows 1, 5 and 10 are compared against experimental data.

Figure 6 shows a contour plot of streamwise velocity along the centreline of the effusion geometry. The jetting region on the upstream wall of each effusion tube can be seen clearly.

The flow in this region has the highest velocity magnitude in the entire domain. It occurs as a result of flow separation that occurs at the inlet of each effusion tube; this is clearly shown by the dark blue contours. As such, the flow slows down on one side of the hole (where the CVP is present) and speeds up on the other side as a result of mass continuity.

An interesting feature of the flow field is the height to which each cooling jet penetrates into the combustor flow. As distance increases in the streamwise direction, the penetration height decreases. This can clearly be seen by the height of the pink jets in Fig. 6. The behaviour of each jet is affected by the flow from upstream jets. At row 1, the exit jet flow, ~12 m/s, is only influenced by the freestream combustor flow which is travelling at ~2.3 m/s. Since the magnitude of velocity exiting the jet is an order of magnitude greater than the freestream flow, the jet is more or less unaffected, thus the height of penetration remains high. At row 5, the freestream flow and the presence of downwash created from the strong CVP of rows 1–4, the flow of which travels between ~6 and 12 m/s, has an increased effect on the penetration height of the jet. It also has an effect on the extent to which the flow bends towards the wall. Both these trends increase with downstream distance since more coolant is injected with each row of holes.

Twelve section planes, aligned normal to the streamwise flow in the combustor, have been created and used to map contours of velocity to illustrate how the flow field develops in the streamwise direction; this is shown in Fig. 7. A section plane was taken through the centreline of each hole (in the spanwise direction) and mirrored about one of the two periodic boundaries, creating the effect of repeating columns.

At the jet hole exit of row 1, it can be seen that the jet has little interaction with the freestream flow. At row 2, the CVP in the main jet from row 1 can be seen as a kidney shape, although not at its maximum penetration height. There still appears to be little interaction between the jets and the free stream flow at this location. At rows 3 and 4, interaction between the jets at rows 1, 2 and 3 compound together and begin to affect the topology of the flow; this is noticeable from the change in velocity near the wall (dark to light blue). The flow field constantly changes as further cooling flow is injected with each row of holes, thus increasing the strength of the vortical structures present. It is clear that the two ‘humps’ created by the CVP of each cooling jet (most noticeable from rows 2 to 8) begin to flatten out after row 8; this is characteristic of the stabilisation of jet mixing effects with increased distance downstream.

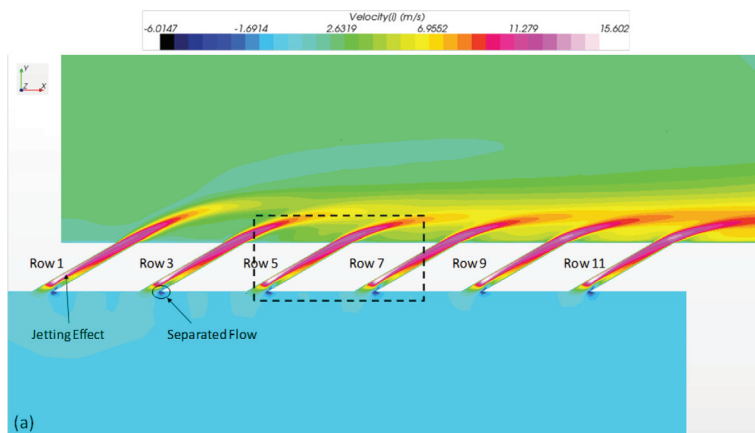


Figure 6: Streamwise velocity contours on the central plane.

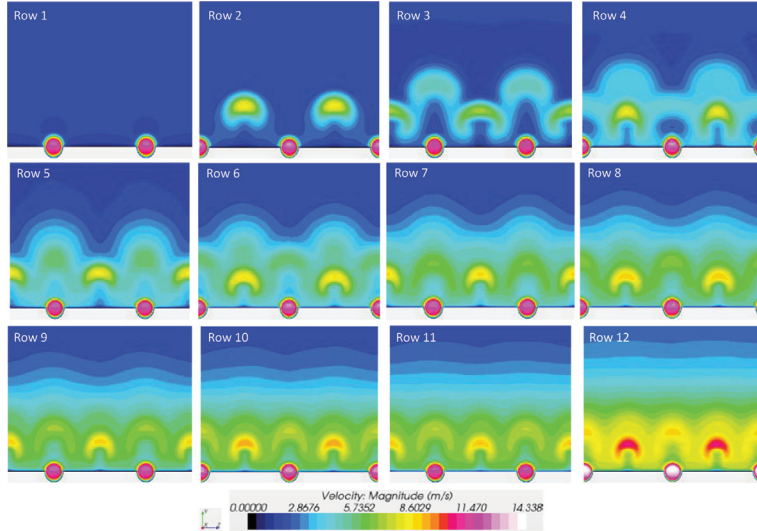


Figure 7: Development of flow field along combustor.

With each row of holes, the velocity of the flow in the lower portion of the combustor (from maximum jet penetration height to the combustor wall) increases; this is due to the addition of cooling flow from each of the upstream jets, which increases the mass flow rate through the combustor. The thickness of this region increases with each row too. It can also be seen that the shape of the main cooling jets becomes narrower and they are bent further towards the wall; this is due to the interaction of CVP from upstream jets.

In a non-isothermal scenario, the faster flow near the combustor wall would correspond to the cooling layer formed by the spreading and mixing of each jet. Figure 7 illustrates that the coolant introduced into the combustor flow with each row of holes would therefore increase the thickness of the cooling layer, thus maximising the life of the combustor wall.

The mean streamwise velocity profiles, measured one cooling row downstream of rows 1, 5 and 10 are presented in Fig. 8(a), (b) and (c) respectively. Each profile is non-dimensionalised by $U_\infty = 2.3$ m/s. It can be seen that as the flow is injected from the first row to the tenth, there is a decrease in the penetration height of the jet, as defined by the maximum streamwise velocity, labelled (1) in Fig. 8(a), (b) and (c). The peak occurs at a height of $\sim 2.4D$ for row 1, $\sim 1.7D$ for row 5 and $\sim 1.4D$ for row 10. The transverse penetration of the jet into the combustor flow and the downstream decay of the streamwise velocity component are evident by tracking this feature over the velocity profiles. It is also interesting to note the region above (1) represents a coalescence of jets from all upstream effusion rows; this results in an increase in the velocity of the outer portion of flow. The contribution of the upstream jets gradually diminishes as the jets decay and spread with increasing streamwise distance. The flow feature labelled (2) in Fig. 8(b) and (c), respectively, is the mean streamwise velocity contribution from the previous row, i.e. row 5 for Fig. 8(b) and row 10 for Fig. 8(c).

The local peak, labelled (3), is a secondary effect resulting from the presence of the primary jet (1). The local maximum (3) is caused by entrainment of the main combustor flow towards the wall. This so-called ‘wall-jet layer’ is generated by longitudinal vortices, which are created at the lateral edges of each cooling hole; these are thought to have the largest

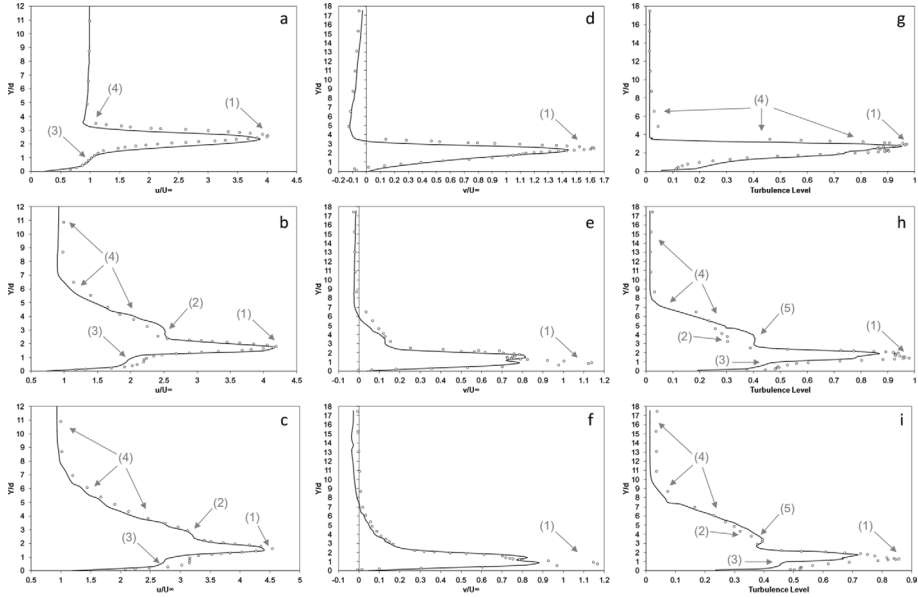


Figure 8: Streamwise velocity profile one hole diameter downstream of row 1 (a), row 5 (b), row 10 (c). Wall-normal velocity profile one hole diameter downstream of row 1 (d), row 5 (e), row 10 (f). Turbulence level profile one hole diameter downstream of row 1 (g), row 5 (h), row 10 (i). Solid line, RST; symbols, experimental data [21].

effect on cooling performance. A negative mean transverse velocity highlights the entrainment of the main flow towards the wall.

As illustrated in Fig. 8(a), the RST model accurately predicts the streamwise velocity profile downstream of row 1. The maximum streamwise velocity (1) and penetration height of the jet are slightly under-predicted. The combustor flow that is entrained by the jet (3) is predicted well. In the transition region between the jet and freestream combustor flow, labelled (4), the velocity is slightly under-predicted. This is thought to be a result of the under-prediction in wall-normal velocity, as illustrated in Fig. 8(d).

Figure 8(b) illustrates that the RST model predicts the streamwise velocity profile downstream of row 5 reasonably well. The maximum streamwise velocity (1) and penetration height of the jet are predicted accurately. The flow that is entrained by the jet (3) is under-predicted and the mean streamwise velocity contribution from the previous row (2) is over-predicted. This is thought to be a result of an underprediction in the mixing of the jets from row 5 and 6. In the region that represents the coalescence of the jets from the previous rows, labelled (4), the velocity of the flow is slightly under-predicted.

Figure 8(c) illustrates that the RST model predicts the streamwise velocity profile downstream of row 10 reasonably well. The maximum streamwise velocity (1) is slightly under-predicted whilst the penetration height of the jet is predicted accurately. The flow that is entrained by the jet (3) is under-predicted more than it was at row 6. The mean streamwise velocity contribution from the previous row (2) is slightly under-predicted, as is the region that represents the coalescence of the jets from previous rows (4).

The difference between the numerical and experimental results may be mainly attributed to poor turbulence modelling in the near wall region.

The wall-normal velocity profile of the flow at rows 2, 6 and 11 is outlined in Fig. 8(d), (e) and (f), respectively. Each profile is non-dimensionalised by $U_\infty = 2.3$ m/s. With the exception of the peak velocity, labelled (1), the RST model predicts the velocity profiles at the three rows reasonably well. At row 2, the wall-normal velocity is under-predicted between $Y/D = 2$ and 5. Upwards of $Y/D = 5$, the velocity profile is over-predicted. This helps to explain the under-prediction of the penetration height of the cooling jet observed in Fig. 8(a). The peak velocity is slightly under-predicted at row 2. Upwards of $Y/D = 2$ at rows 6 and 11, the RST model slightly under-predicts the wall-normal velocity profile.

A double velocity peak occurs between $Y/D = 0$ and 2. Although the RST model vaguely captures two peaks, it fails to predict the correct profile and magnitude of the velocity peaks. This may be related to the turbulence modelling near the wall.

The negative wall-normal velocity profile close to the wall is not predicted by the RST model. This is considered to be due to the fact that only two very thin prism layers were used near the wall. To improve the wall-normal velocity profile in the near wall region, and perhaps the velocity magnitude of the entrained fluid, a thicker prism mesh, with more than two prism layers, should be incorporated. However, due to the sharp angle of each effusion tube this is difficult to incorporate since cells with high aspect ratios and skewness are generated.

Turbulence level (TL) is defined as $TL = \left(\sqrt{0.5(u_{rms}^2 + v_{rms}^2)} / U_{local} \right)$. Turbulence profiles measured one hole diameter downstream of rows 1, 5 and 10 are presented in Fig. 8(g), (h) and (i), respectively. Distinct regions in the turbulence level profiles correspond to complex features within the flow field. The peak turbulence level of each jet, labelled (1), is consistent with the shear layer at the bottom of the coolant jet. The minima, labelled (2), corresponds to a near-zero streamwise velocity gradient at that location. The drop in turbulence level near the wall, labelled (3), corresponds to the secondary velocity peak at that location. The region labelled (4) corresponds to the outer flow region which is affected by the coalescence of upstream jets.

The turbulence level profile predicted by the RST model is reasonable. The peak magnitude of turbulence level (1) is predicted correctly at row 2 but is under-predicted at rows 6 and 11. At rows 2 and 6, the double peak in turbulence level is not predicted well by the RST model. At row 11, the shape of the peak, although under-predicted in magnitude, is quite representative of the experimental data. The minima labelled (2) is significantly under-predicted at row 6 but predicted well at row 11; this may be linked to the fact that jet interactions become more stable with downstream distance. As with the streamwise velocity profiles, the turbulence levels in the region of entrainment (3) are slightly under-predicted at rows 6 and 11. The turbulence level profile in region (4) is under-predicted at each row. This along with the over-prediction of the local maxima labelled (5) in Fig. 8(h) and (i) is most likely the reason that the streamwise velocity profile is also predicted incorrectly in these regions.

The overall under-prediction in the turbulence level profiles is perhaps linked to the fact that the current simulation was based on a steady flow analysis. In reality, the effusion flow case is unsteady due to the continuous injection of coolant over many rows thus simulating the flow field using a time-dependant analysis, such as LES, should improve the accuracy of the results but the computational cost would increase significantly too.

3.2 Non-isothermal simulation

A contour plot of temperature along the centre plane of the domain is shown in Fig. 9 and the heat transfer throughout the effusion plate is clearly visible. The conduction zone, upstream of row 1 and the high jet penetration of row 1 can also be clearly seen in this figure.

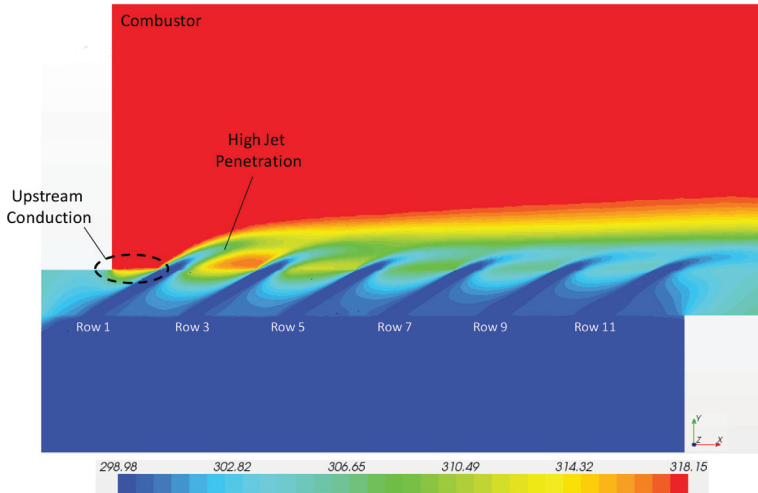


Figure 9: Temperature contours on the central plane.

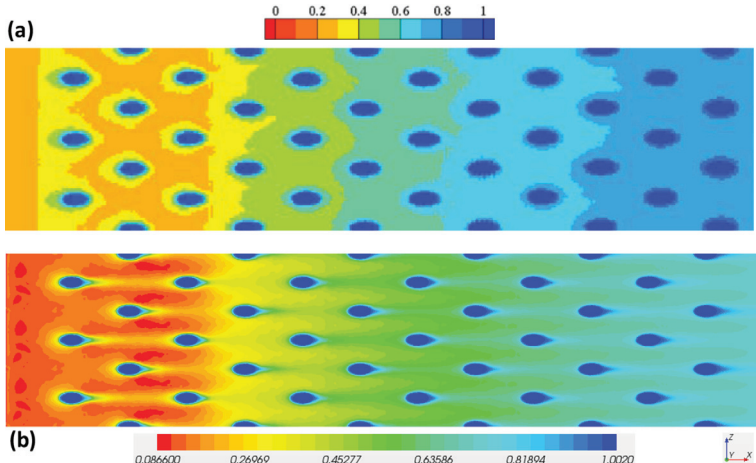


Figure 10: Cooling effectiveness contours of the effusion plate from rows 1 to 12: (a) experiment and (b) simulation.

Figure 10 presents a qualitative comparison between the predicted cooling effectiveness and the measurements. In general, the predicted cooling effectiveness contour is matched reasonably well to the experimental contour and the conduction zone upstream of row 1 as mentioned above is also evident from the non-zero cooling effectiveness levels at the leading edge of the first row of holes. This conduction can be explained by the fact the cooling holes are cooling the plate through convection within the holes.

To quantify exactly how the cooling performance between the experiment and RST simulation compares, Fig. 11 shows the laterally averaged cooling effectiveness, starting from the leading edge of the first row of holes ($X/S_s = 0$, X is the distance from the leading edge of the first row of holes and S_s is the streamwise hole spacing) and finishing one streamwise hole pitch downstream of row 12.

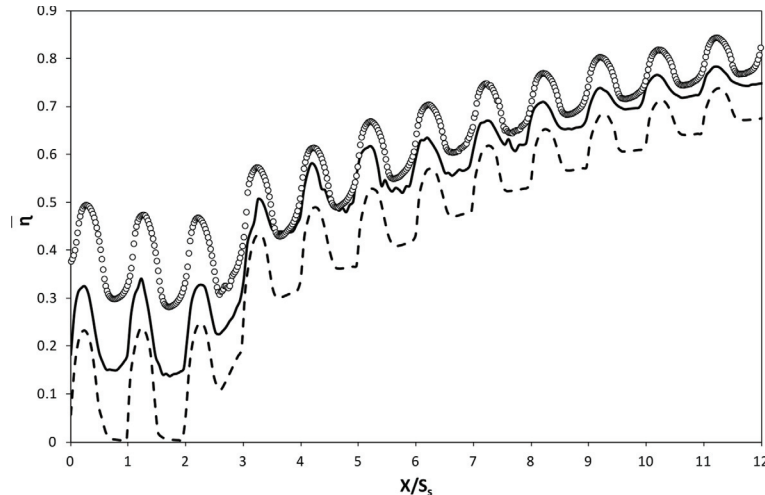


Figure 11: Laterally averaged cooling effectiveness over rows 1 to 12. Solid line, RST (with CHT); dashed line, RST (without CHT); symbols, experimental data.

Overall, the laterally averaged cooling effectiveness predicted by the RST simulation matches the experimental results reasonably well. The overall trend, i.e. the initial decrease of $\bar{\eta}$ over the first three rows, followed by a gradual increase in $\bar{\eta}$ over the remaining nine rows is predicted correctly. The general increase in $\bar{\eta}$ from rows 4 to 12 is characteristic of the fact that with every row, coolant is injected and due to the interaction of CVP of each jet with the downstream flow, the cooling flow is entrained further downstream and pushed closer to the wall, meaning the wall is cooled more effectively; this effect takes several rows to occur since the jet mixing effects take time to become stable.

The decrease in cooling effectiveness from $X/S_s = 0$ to $X/S_s = 2$ (the leading edge of row 3) before an increase is observed is most likely due to the fact the jet penetration height in this region is high which means the coolant does not effectively cool the plate until further downstream where the velocity peaks move closer to the wall. It is also likely the jets in this region entrain hot mainstream flow to the surface by the longitudinal vortices, preventing the wall from being cooled properly.

The laterally averaged cooling effectiveness appears to oscillate over the effusion plate; this is because the measurements taken over the entire plate also include the flow at the exit of each cooling jet where $\bar{\eta} = 1$, thus increasing the spanwise average of η . In regions away from the jet exits $\bar{\eta}$ is lower which results in a lower spanwise average.

The oscillating nature of $\bar{\eta}$ is correctly predicted over the plate but the magnitude of the peaks and troughs are slightly underpredicted. First, it is noticeable that from rows 1 to 3 ($X/S_s = 0\text{--}2$), the magnitude of $\bar{\eta}$ is underpredicted by approximately 35%. The underprediction of $\bar{\eta}$ is most likely due to an underprediction of the lateral spreading and mixing of the jets in this region, thus the wall of the combustor is not cooled as effectively as it should be.

Whilst the overall increasing trend in $\bar{\eta}$ is predicted when the plate is not modelled (dashed line in 11), it can clearly be seen that the magnitude of $\bar{\eta}$ is significantly underpredicted (max $\Delta\eta = 0.29$ at $X/S_s \sim 2$ and min $\Delta\eta = 0.12$ at $X/S_s \sim 11$) across the entire plate. This confirms that adopting a CHT approach in effusion cooling scenarios is essential to accurately predict the cooling performance and heat transfer characteristics.

4 CONCLUSIONS

This paper describes a CFD study of effusion cooling flow and heat transfer. In the isothermal study, the predicted mean streamwise velocity profiles at all three locations (rows 2, 6 and 11) match the experimental measurements well. With the exception of the single peak at row 2 and double peaks at rows 6 and 11, the predicted wall-normal velocity profiles agree reasonably well the experimental data. At row 2, the single peak velocity is slightly under-predicted and the double velocity peaks at rows 6 and 11 are poorly captured by the RST model. The turbulence level profiles at rows 2, 6 and 11 are satisfactorily predicted. The peak turbulence level is correctly predicted at row 2 but under-predicted at rows 6 and 11.

In the non-isothermal study, the predicted laterally averaged cooling effectiveness matches the experimental measurements reasonably well. The overall trend, i.e. the initial decrease of $\bar{\eta}$ over the first three rows, followed by a gradual increase in $\bar{\eta}$ over the remaining nine rows is predicted correctly. The largest under-prediction is observed from rows 1 to 3. In this region, it is possible that the entrainment of flow is predicted incorrectly and so the jets entrain hot mainstream flow to the surface by the longitudinal vortices, preventing the wall from being cooled properly. From rows 4 to 12, the under-prediction in the magnitude of $\bar{\eta}$ could be linked to an under-prediction of the entrainment of cooling flow downstream and towards the combustor wall which will result in lower cooling efficiency.

Whilst the overall increasing trend in $\bar{\eta}$ is predicted, it is clear that the magnitude of $\bar{\eta}$ is significantly underpredicted across the entire effusion plate when the plate itself is not included in the simulation, i.e. no CHT approach is adopted. The importance of adopting a CHT approach in effusion cooling scenarios is confirmed by the under-prediction of $\bar{\eta}$ observed from the non-CHT-based simulation.

REFERENCES

- [1] MacManus, D.G. & Eaton, J.A., Flow physics of discrete boundary layer suction – measurements and predictions. *Journal of Fluid Mechanics*, **417**, pp. 47–75, 2000. doi: <http://dx.doi.org/10.1017/s0022112000001026>
- [2] Peterson, S.D. & Plesniak, M.W., Evolution of jets emanating from short holes into cross flow. *Journal of Fluid Mechanics*, **503**, pp. 57–91, 2004. doi: <http://dx.doi.org/10.1017/s0022112003007407>
- [3] Walters, D.K. & Leyklek, J.H., A detailed analysis of film-cooling physics. Part I: streamwise injection with cylindrical holes. *ASME Journal of Turbomachinery*, **122**, pp. 102–112, 2000. doi: <http://dx.doi.org/10.1115/1.555433>
- [4] Bazdidi-Tehrani, F. & Andrews, G.E., Full-coverage discrete hole film cooling: investigation of the effect of variable density ratio. *Journal of Engineering for Gas Turbines and Power*, **116**, pp. 587–596, 1994. doi: <http://dx.doi.org/10.1115/1.2906860>
- [5] Crawford, M.E., Kays, W.M. & Moffat, R.J., Full-coverage film cooling. Part I: comparison of heat transfer data for three injection angles. *Journal for Engineering for Power*, **102**, pp. 1000–1005, 1980. doi: <http://dx.doi.org/10.1115/1.3230334>
- [6] Metzger, D.E., Takeuchi, D.I. & Kuenstler, P.A., Effectiveness and heat transfer with full-coverage film-cooling. *Journal for Engineering for Power*, **95**, pp. 180–184, 1973. doi: <http://dx.doi.org/10.1115/1.3445720>
- [7] Martinez-Botas, R.F. & Yuen, C.H.N., Measurement of local heat transfer coefficient and film cooling effectiveness through discrete holes. *ASME Turbo Expo 2000-GT-243*, 2000. doi: <http://dx.doi.org/10.1115/2000-gt-0243>
- [8] Lin, Y., Song, B., Li, B., Liu, G. & Wu, Z., Investigation of film cooling effectiveness of full-coverage inclined multihole walls with different hole arrangements. *ASME Turbo Expo GT2003-38881*, 2003. doi: <http://dx.doi.org/10.1115/gt2003-38881>

- [9] Facchini, B., Maiuolo, F., Tarchi, L. & Coutadin, D., Combined effect of slot injection, effusion array and dilution hole on the heat transfer coefficient of a real combustor liner – Part 1: experimental analysis. *ASME Turbo Expo GT2010-22936*, 2010. doi: <http://dx.doi.org/10.1115/gt2010-22936>
- [10] Ligrani, P., Goodro, M., Fox, M. & Moon, H-K., Full-coverage film cooling: film effectiveness and heat transfer coefficients for dense and sparse hole arrays at different blowing ratios. *Journal of Turbomachinery*, **134**, pp. 061039-1–061039-13, 2012. doi: <http://dx.doi.org/10.1115/1.4006304>
- [11] Andreini, A., Caciolli, G., Facchini, B. & Tarchi, L., Experimental evaluation of the density ratio effects on the cooling performance of a combined slot/effusion combustor cooling system. *ISRN Aerospace Engineering*, 2013, Article ID 423190, pp. 1–14, 2013. doi: <http://dx.doi.org/10.1155/2013/423190>
- [12] Krewinkel, R., 2013, A review of gas turbine effusion cooling studies. *International Journal of Heat and Mass Transfer*, **66**, pp. 706–722, 2013. doi: <http://dx.doi.org/10.1016/j.ijheatmasstransfer.2013.07.071>
- [13] Mendez, S., Nicoud, F. & Poinsot, T., Large-eddy simulations of a turbulent flow around a multi-perforated plate. *Complex Effects in LES*, **56**, pp. 289–303, 2006. doi: http://dx.doi.org/10.1007/978-3-540-34234-2_21
- [14] Bennett, W.P., Yang, Z. & McGuirk, J.J., Isothermal study of effusion cooling flows using a large-eddy simulation approach. *Journal of Aerospace Power*, **24**, pp. 729–939, 2009.
- [15] Berhe, M.K. & Patankar, S.V., Curvature effects on discrete-hole film cooling. *Journal of Turbomachinery*, **121**, pp. 781–791, 1999. doi: <http://dx.doi.org/10.1115/1.2836732>
- [16] Lakehal, D., Theodoridis, G.S. & Rodi, W., Computation of film cooling of a flat plate by lateral injection from a row of holes. *International Journal of Heat and Fluid Flow*, **19**, pp. 418–430, 1998. doi: [http://dx.doi.org/10.1016/s0142-727x\(98\)10022-x](http://dx.doi.org/10.1016/s0142-727x(98)10022-x)
- [17] York, W.D. & Leylek, J.H., Numerical prediction of mainstream pressure gradient effects in film cooling. *ASME Paper 99-GT-166*, 1999.
- [18] Jansson, L.S. & Davidson, L., Numerical simulation of inclined jets in a crossflow using a Reynolds stress model. *Proceedings 2nd European Computational Fluid Dynamics '94*, pp. 535–542, 1994.
- [19] Jansson, L.S. & Davidson, L., Numerical study of effusion cooling in a double-row discrete-hole configuration using a low-Re Reynolds stress transport model. *Engineering Turbulence Modelling and Experiments*, **3**, pp. 731–740, 1996. doi: <http://dx.doi.org/10.1016/b978-0-444-82463-9.50076-9>
- [20] Gustafsson, K.M.B. & Johansson, T.G., Numerical simulation of effusion cooling with comparisons to experimental data. *Progress in Computational Fluid Dynamics*, **6**, pp. 101–109, 2006. doi: <http://dx.doi.org/10.1504/pcfd.2006.009487>
- [21] Scrittore, J., Experimental study of the effect of dilution jets on film cooling flow in a gas turbine combustor. *PhD Thesis*, Virginia Polytechnic Institute and State University. Blacksburg, 2008.
- [22] Daly, B.J. & Harlow, F.H., Transport equations in turbulence. *Physics of Fluids*, **13**, pp. 2634–2649, 1970. doi: <http://dx.doi.org/10.1063/1.1692845>
- [23] Gibson, M.M. & Launder, B.E., Ground effects on pressure fluctuations in the atmospheric boundary layer. *Journal of Fluid Mechanics*, **86**, pp. 491–511, 1978. doi: <http://dx.doi.org/10.1017/s0022112078001251>
- [24] Silietti, M., Kassab, A. & Divo, E., Film cooling effectiveness: comparison of adiabatic and conjugate heat transfer CFD models. *International Journal of Thermal Sciences*, **48**, pp. 2237–2248, 2009. doi: <http://dx.doi.org/10.1016/j.ijthermalsci.2009.04.007>